

INTRODUCTION/INSTRUMENT

Introduction

The Electron Spectrometer (ELS), flown on the ESA Mars Express (MEx) spacecraft as part of the Analyzer of Space Plasmas and Energetic Atoms (ASPERA-3) experiment [Barabash *et al.*, 2004, 2006], has been studying electron plasma since 2004. To date, ELS continues to measure *in situ* electron plasma in the Mars environment and solar wind.

The MEx spacecraft samples data from an elliptical orbit (250 x 10,000 km) with a quasi-polar inclination of $\sim 86.5^\circ$. To date, the periapsis of the spacecraft increased from 250 km to its present periapsis of 380 km, the inclination drifted to $\sim 87^\circ$, and the orbital period lengthened by ~ 0.5 hours, yielding about three orbits of Mars per Earth day. The latitude of pericenter drifts to cover the globe and the orbit plane precesses in longitude providing full global coverage in ~ 1 Earth year.

During observations of the Martian electron environment, the ELS instrument experienced several different types of contamination that altered the electron spectrum from Mars. These signals include external fluxes due to penetrating radiation caused by geophysical events like solar energetic particle (SEP) events, cosmic rays that penetrate through the instrument, thermal noise generated within the ELS microchannel plate (MCP), outgassing of the MCP, and electronic noise. All these sources result in events that trigger the MCP, generating counts which are independent of the instantaneous energy band pass (energy independent), creating contamination to the measurement of Mars' plasma; however, these sources are time dependent. The contamination distorts the measured electron spectrum, making it difficult to determine the true interaction of the planet during these times.

Because these contamination events can occur on different time scales, determining a method for removal of the background contamination was developed over a period of time. Frahm *et al.* [2013a,b] developed a 5-minute average background removal which was applied to a SEP event occurring on 27 January 2012, see Figure 1. Applying background removal uncovered how the electron spectrum at Mars changed during this SEP event. The time cadence of 5-minute averages was chosen to match the background rates determined for the Electron Reflectometer flown on the Mars Global Surveyor, so that similar comparisons of backgrounds could be made [Delory *et al.*, 2012]. The method for determining the ELS Background uses spectral data above 10 keV. A discussion of background corrections may be found in Frahm [2021].

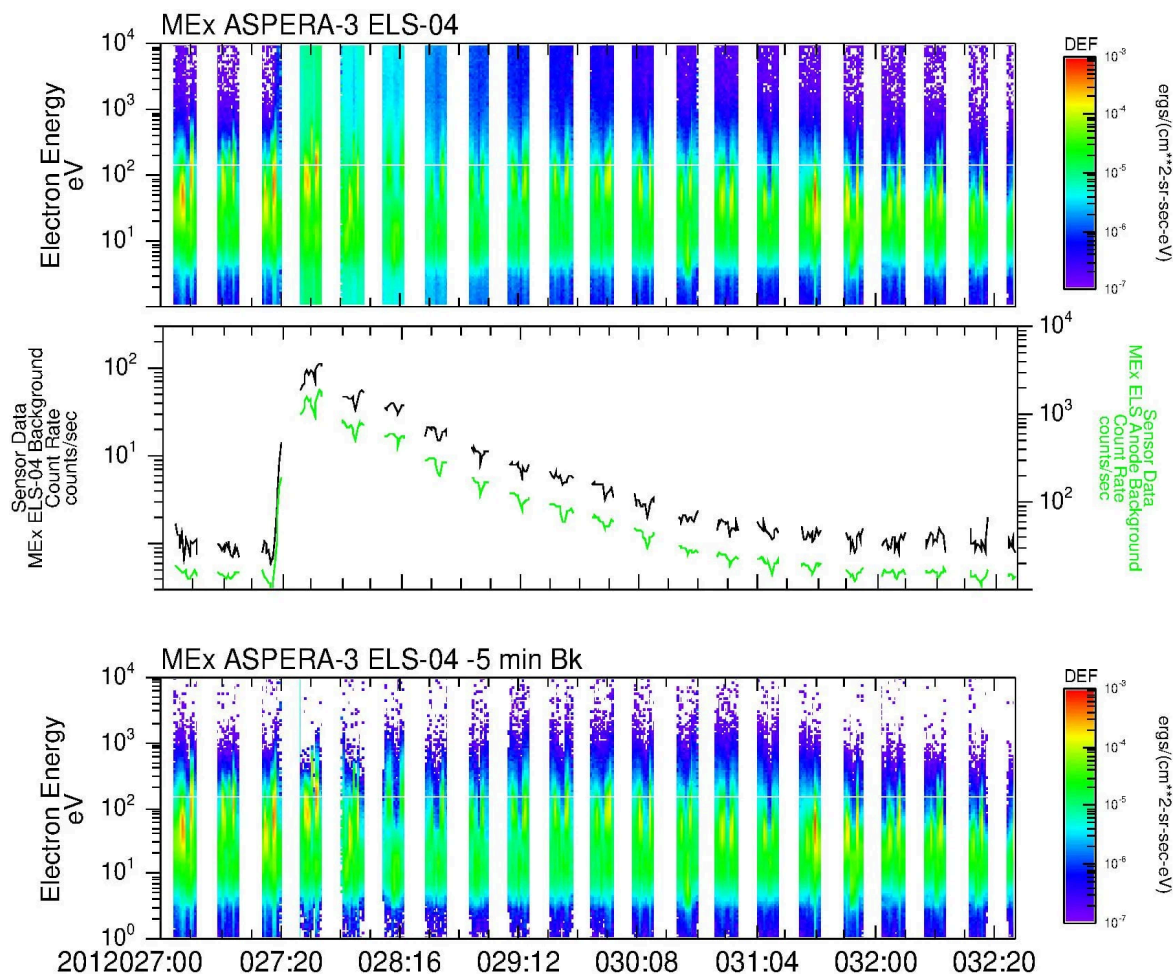


Figure 1. The top and bottom spectrograms show the ELS spectra before and after background correction due to an SEP event. Background count rates (center panel) show the time profile of the influence of the SEP event (for ELS-04 on left in black and total MCP background counts on right in green). Note: scales differ). Horizontal gaps represent times when the instrument is off.

Between 2013 and 2018 additional time cadence backgrounds of instrument sampling rate (4 sec), 1-minute averages, and 25-minute averages were developed, driven by various plasma boundary and plasma studies [Duru *et al.*, 2017, Frahm *et al.*, 2018, Möstl *et al.*, 2015, Posner *et al.*, 2013, Rollett *et al.*, 2014]. NASA made the decision to stop funding U.S. Mars Express activities, so archiving of this data could not be done. However, the ELS background data continues to be used by the science community [Duru *et al.*, 2023, Harada *et al.*, 2024, Madanian *et al.*, 2024], so NASA awarded this ROSES PDART grant to archive the ELS background data within the NASA Planetary Plasma Interaction (PPI) node of the Planetary Data System (PDS) in PDS-4 compliant format and make it publically available.

Instrument

A cross-sectional view of the MEx ELS sensor is shown in Figure 2. Normally, plasma enters ELS through an inlet opening in the side of the detector housing from an azimuth of 360° . This azimuth is segmented into 16 sectors, each 22.5° wide (numbered 0-15). The elevation acceptance angle is $\pm 2^\circ$. The entering plasma passes through the collimator, where the plasma from angles beyond the acceptance range is removed. Plasma then enters the top hat region where spherical deflection plates separate out the electron plasma of specific energy using an electric field generated from either of two power supplies covering the low range (LR) energy (0.5 eV to ~ 150 eV) and the high range (HR) energy

(~150 eV to ~20 keV). The selected electrons are then focused on to a microchannel plate (MCP) sensor. The electron signal is multiplied by the MCP, passed to an anode where electrons are collected, amplified by a charge sensitive amplifier, and counted.

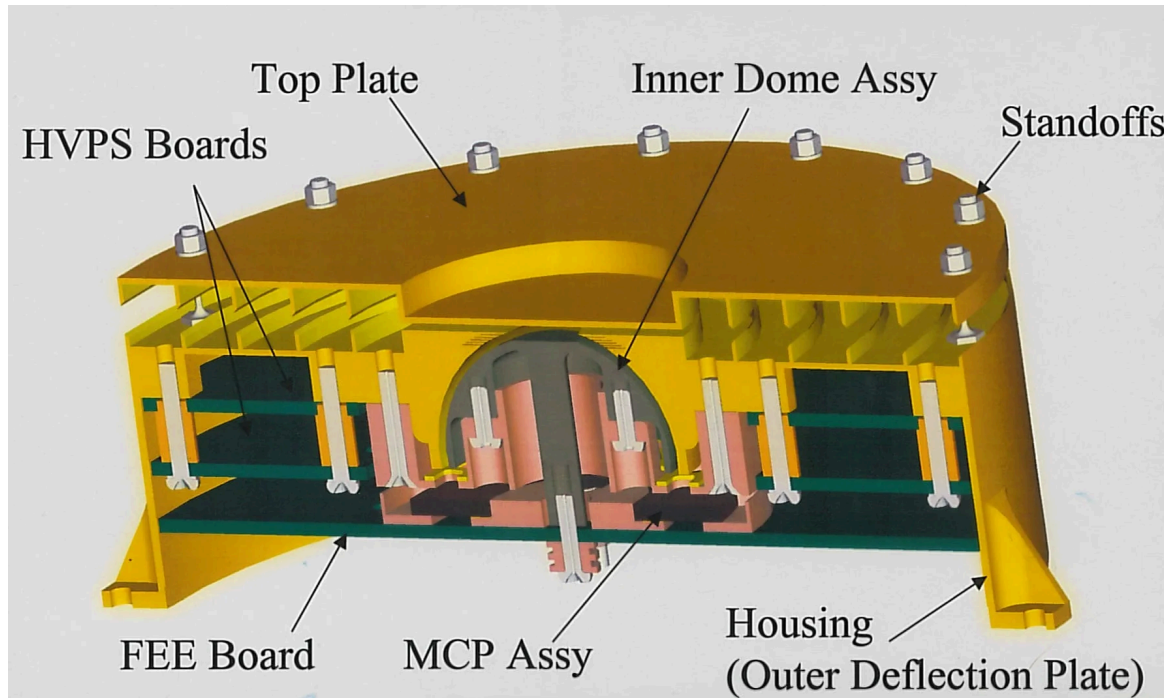


Figure 2. Cross-section of the SES instrument showing the internal geometry. Plasma enters through the sides of the housing and travels between the collimator baffles which refine the plasma into a beam. Two programmable power supplies (PPS) generate an electric field between the top plate/outer plate and the inner dome which selects electrons. Energy selection occurs further as the electrons travel between the inner and outer domes, eventually striking the MCP assembly where they are magnified and turned into an electronic signal by the front-end electronics (FEE). The MCP voltage is determined by a separate high voltage power supply (HVPS) to keep the MCP efficiency at peak performance. Contamination protection by ultraviolet light (UV) is achieved by baffles in the collimator and light traps at the entrance to the deflection domes.

The ASPERA-3 ELS data stored at PDS include both raw and calibrated forms. The "calibrated" designation means that the data values account for instrument parameters and the value produced has been reconstructed correctly to give an accurate representation of the measurement in geophysical units. Different effects observed in the data are often adjustments to the calibrated values to remove known phenomena and produce a higher-level data product. Such is the case for background effects observed within the ELS. The PDS calibrated ELS data contains both the environment plasma signal and signals generated internal to the instrument. In the ELS documentation, there is no discussion or description of signals from penetrating radiation, or guidance on how to recover the environmental signal from the ELS data because at the time of data submission, no sources of contamination were identified.

NOISE BACKGROUND CORRECTION

Background Correction

Removal of the energy independent background component in the spectrum can cause significant adjustments. Figure 3 contains a spectrum during the peak of the SEP event shown in Figure 1, when the spacecraft was in the solar wind. The energetic particles penetrate through the sides of the detector and produce a signal which is independent of the energy of the electrons being measured instead of traveling through the collimator and following the flight path through the instrument. This contamination signal generates a constant level of noise which is the same throughout the energy sweep, equally contaminating measurements at high energies as well as low energies. Here the background level is generated every 4 sec to cope with the high contamination rates and the fast variability that the SEP causes.

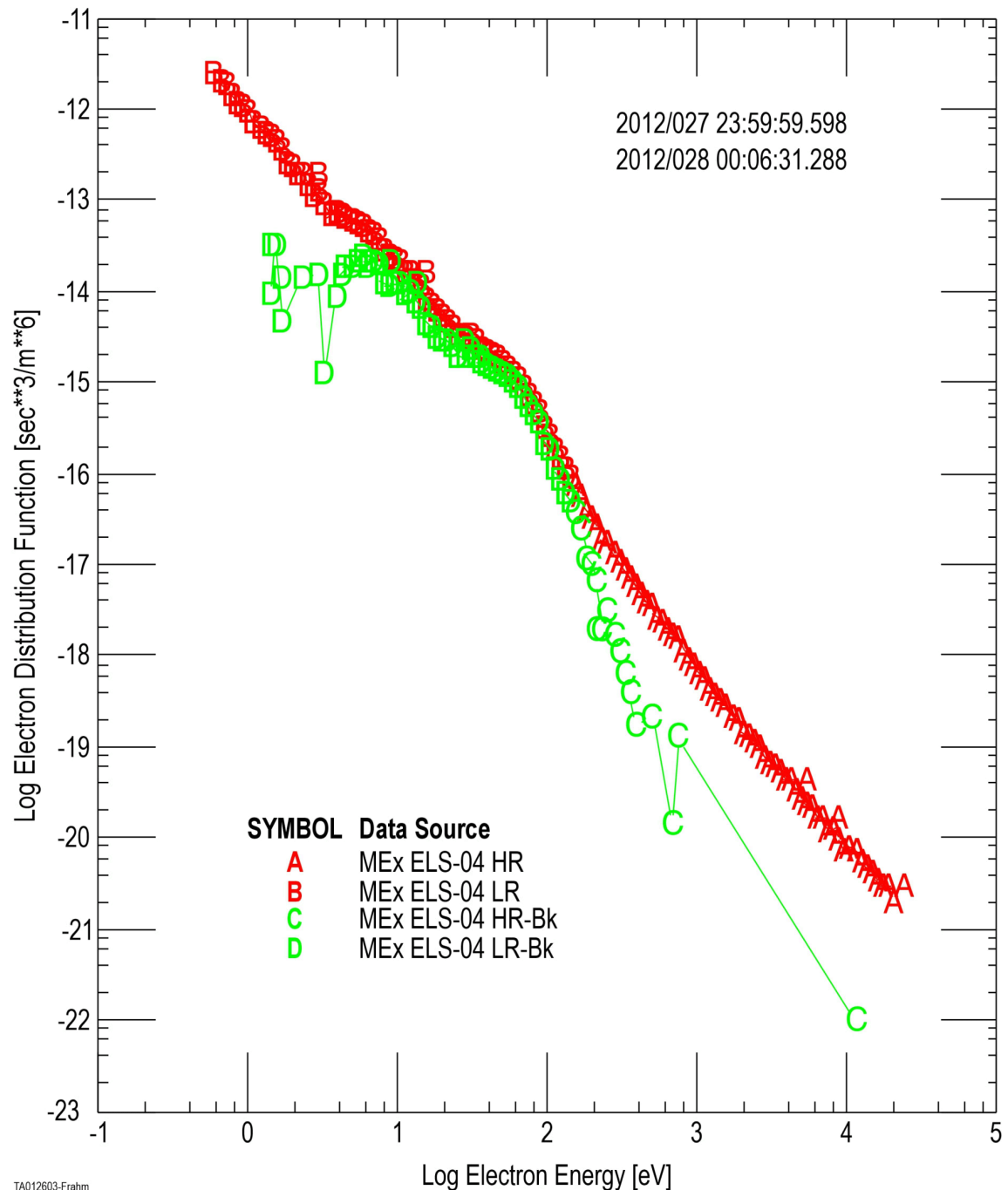


Figure 3. Solar wind electron spectrum before and after a 4-second background correction showing the influence at all energies with the large and the small energies affected the most. Red-original uncorrected. Green-background removed.

There are times when the background level in some sectors can be high at the same time other sectors show a low background. This can be seen in Figures 4 and 5. Figure 4 shows a time period where there are high levels of noise which exist only in part of the instrument. This can be caused by electrical or sensor specific noise; however, this noise is energy independent, so the same technique can be used to remove noise keeping in mind that the background level is sector dependent.

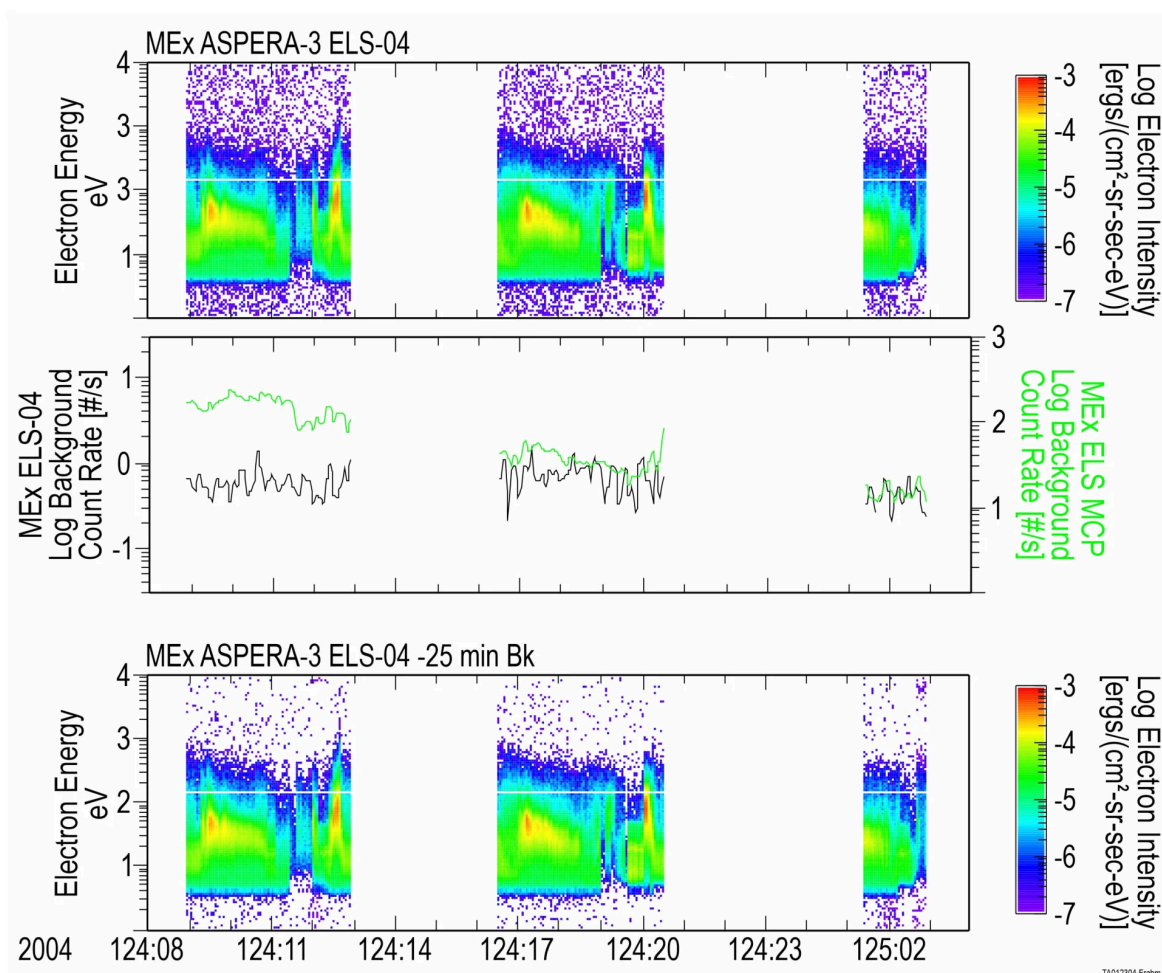


Figure 4. Example of a quiet ELS sector at the same time other parts of ELS are exhibiting noise. Sector 04 shows a 3-orbit time span when the anode sum background value in part of ELS is elevated, while at the same time, the background noise remains steady in ELS sector 04. Since ELS sector 04 is quiet, a 25-minute average background calculation is the appropriate quantity to remove. The bottom panel shows the result of removing the 25-minute background from the original spectra shown in the top panel (Same format as Figure 1).

Figure 5 shows the same 3-orbit time as Figure 4, but for sector 01. The background noise in sector 01 changes much faster and requires a faster changing background, designed for a more intense time. Thus, to recover the true spectrum requires removal a 1 min average background.

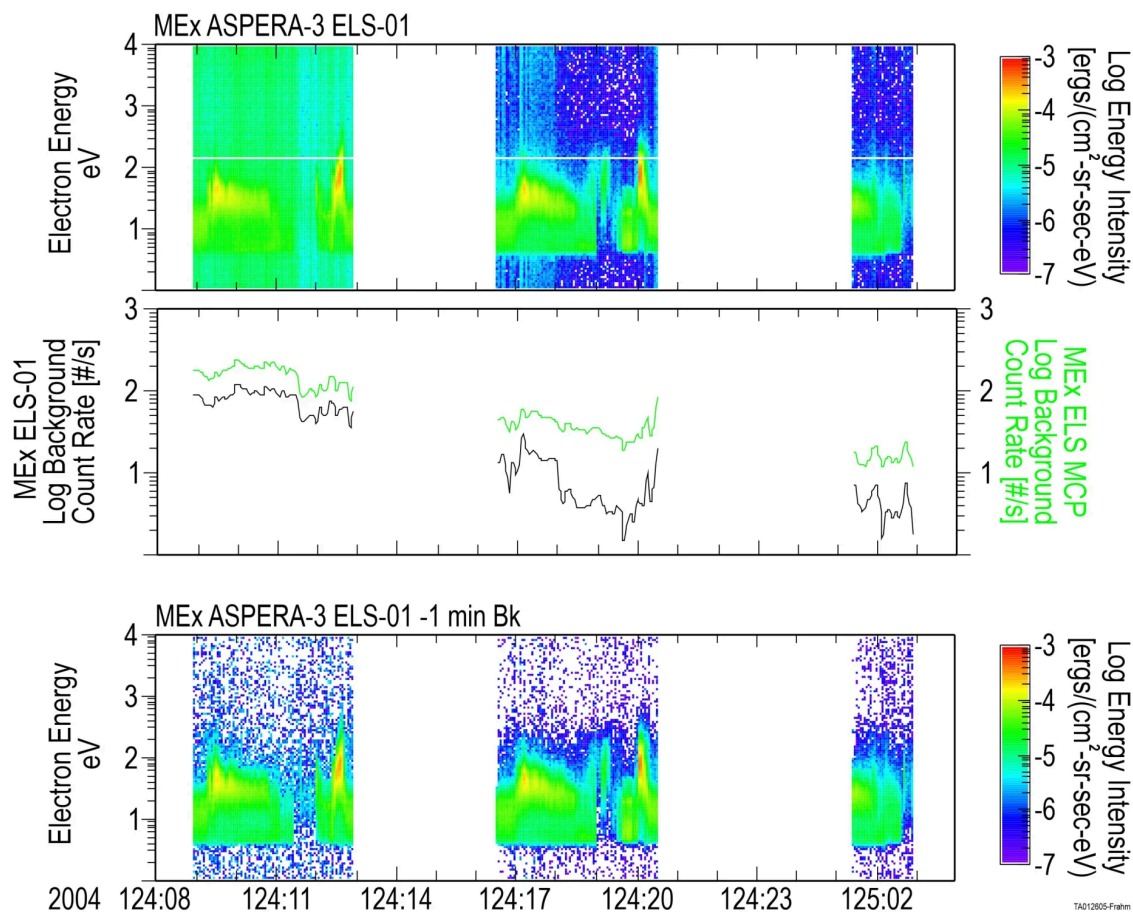


Figure 5. A noisy ELS sector at the same time other sectors are quiet. Sector 01 shows the same 3-orbit time span as Figure 4 when background for sector 01 is elevated and sector 04 remained quiet. A 1-minute average background is appropriate to remove for the noisy sector 01. The 1-minute background is removed (bottom panel) from the original spectra (top panel).

In the above examples, one type of background resolution is applied to the entire measurement at one time. Even though there can be different time resolutions which have different background values for each ELS sector, different time resolutions of background subtraction need to be applied to different sectors at the same time as indicated by Figures 4 and 5.

Variable Background Subtraction

The most appropriate background level balances the ability to change values at the appropriate cadence along with the amplitude of the background. If the value of background changes too quickly, background may remove critical features in the data; however, if the background changes too slowly, the final data at the edges of the background cadence may have too little or too much background removed. To balance the type of background removed from the science data, we need to balance the statistics of each background type. This occurs when the background count frequency matches at two time resolutions. This is shown in Table 1. The matching count level is highlighted in red where the maximum frequency of the longer duration background type matches the minimum frequency for the shorter duration background type as shown by the last columns.

Background Type	Transition Count				Frequency Range	
	4 second	1 minute	5 minute	25 minute	Maximum	Minimum
4 second	6	-	-	-	117 kHz	21.4 Hz
1 minute	90	20	-	-	21.4 Hz	5.42 Hz
5 minute	450	100	20	-	5.42 Hz	1.08 Hz
25 minute	2250	500	100	1	1.08 Hz	0.0108 Hz

Table 1. Optimal Background. For each background level, the background transition count and frequency range where the switch occurs from one level to the next finer resolution level is given.

Using the requirements shown in Table 1, a background product was created which combines all four background resolutions to automatically use the most appropriate type of background. This product balances the accumulation time and amplitude which allows the selection of the best available background type to remove from the science data. Figure 6 shows the result of using this combined background type against the science data presented in Figure 1.

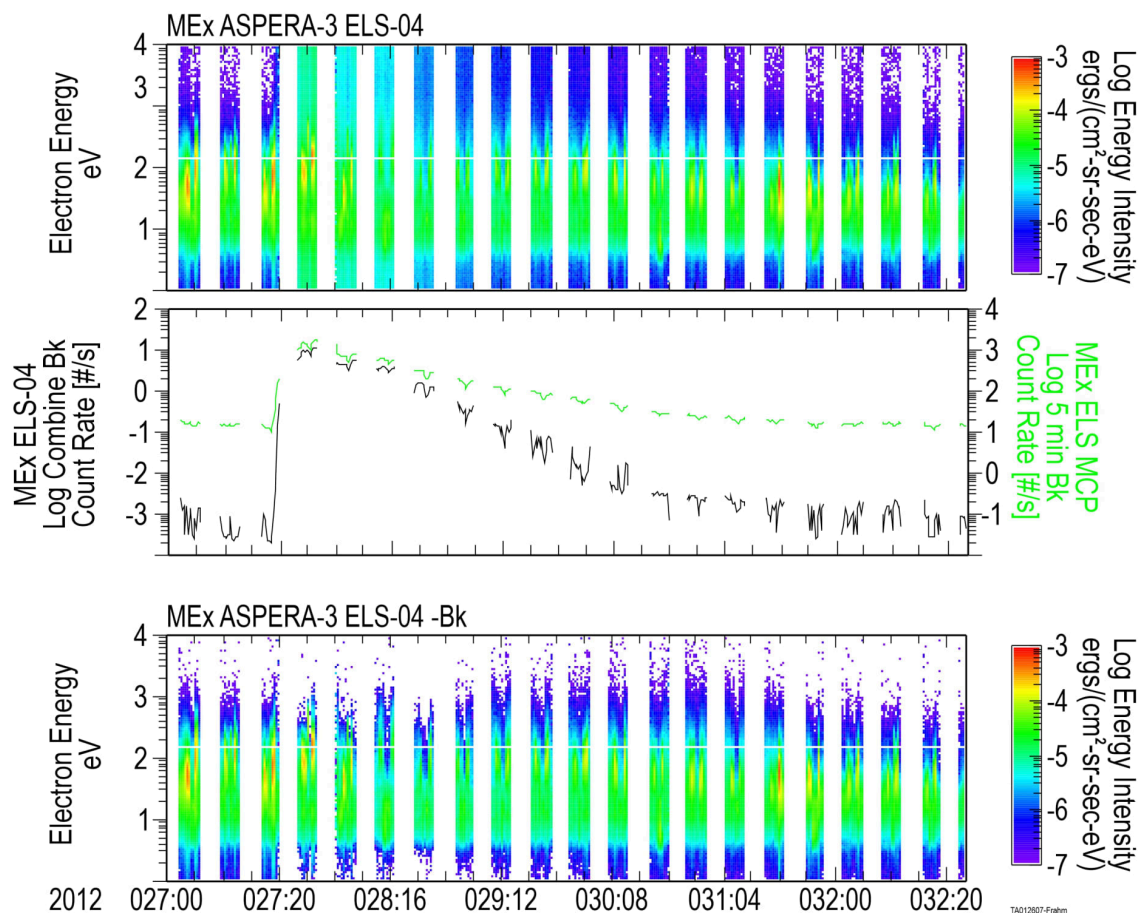


Figure 6. The multi-source combined background data is applied to the measured science data. The format is the same as in Figure 1. The science data, shown in the lower panel after the background has been removed, indicates lower energy intensity at higher energy in the solar wind, but similar energy intensities at higher energies in the magnetosheath.

WHAT IS REVEALED

What Background Subtraction Reveals

Not all SEP events have the same time profile. Figure 7 shows an SEP event which occurred in 2011. In the original science data, a rise in the high energy flux a day before the SEP event is observed and that is not observed when the SEP contacts Mars in the 2012 event. However, there is an extended period where the SEP inflates the Mars magnetosheath in 2011 which is opposite to what was observed in the 2012 storm shown in Figure 6. In addition, there is a higher energy solar wind flux and a greater intensity of the sheath which gradually subsides, also opposite of the 2012 SEP event where the levels are about constant.

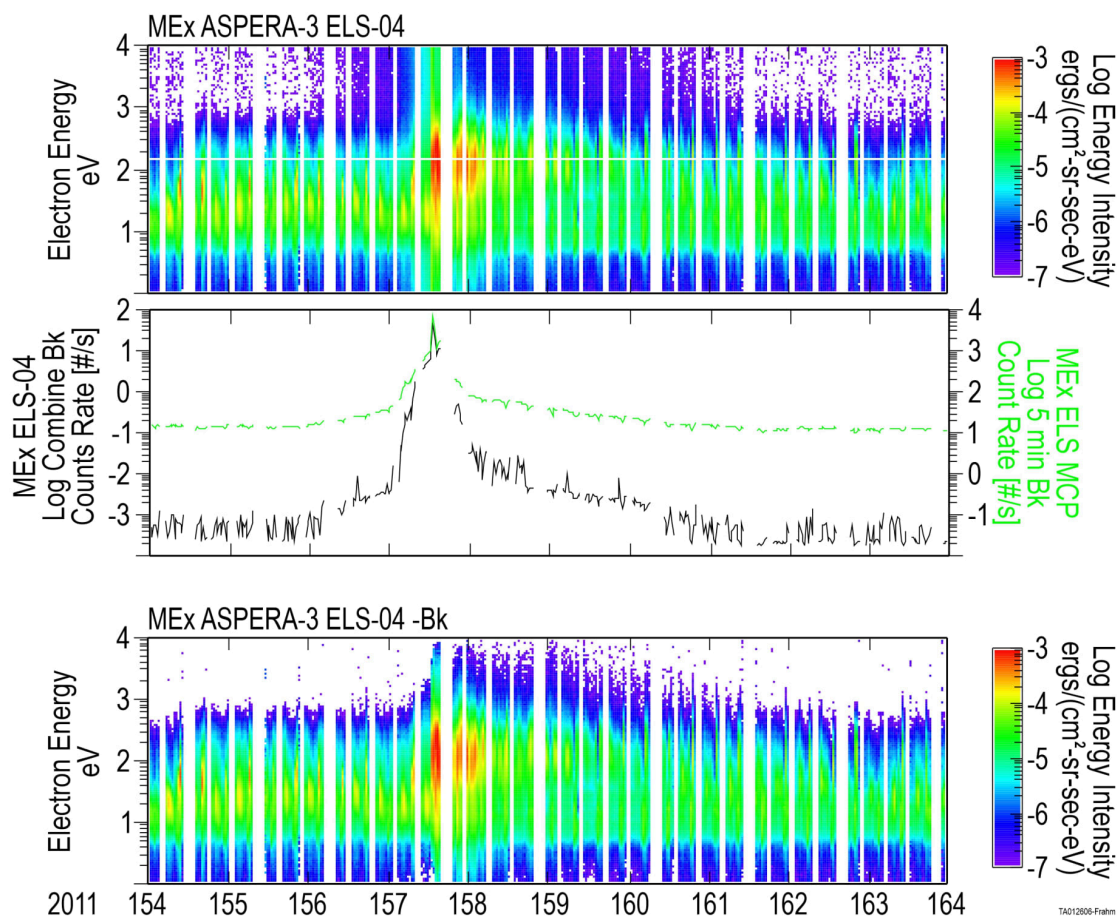


Figure 7. SEP event occurring in 2011. The rise in background flux (second panel) is not observed once the multi-time resolution combined background corrections are made. No dip in solar wind flux at higher energies and no decrease in peak magnetosheath energy is observed. The format is the same as in Figure 6.

Not all solar storms have a short time scale rise in energy intensity at high energy. Figure 8 shows a time in 2014 when there exists an increase in the high energy background, but there is no short time scale rise in the background. The multi-time resolution background subtraction shows that there is also an increase in the solar wind energy flux at high energies and there are some increases in the magnetosheath energy flux as well.

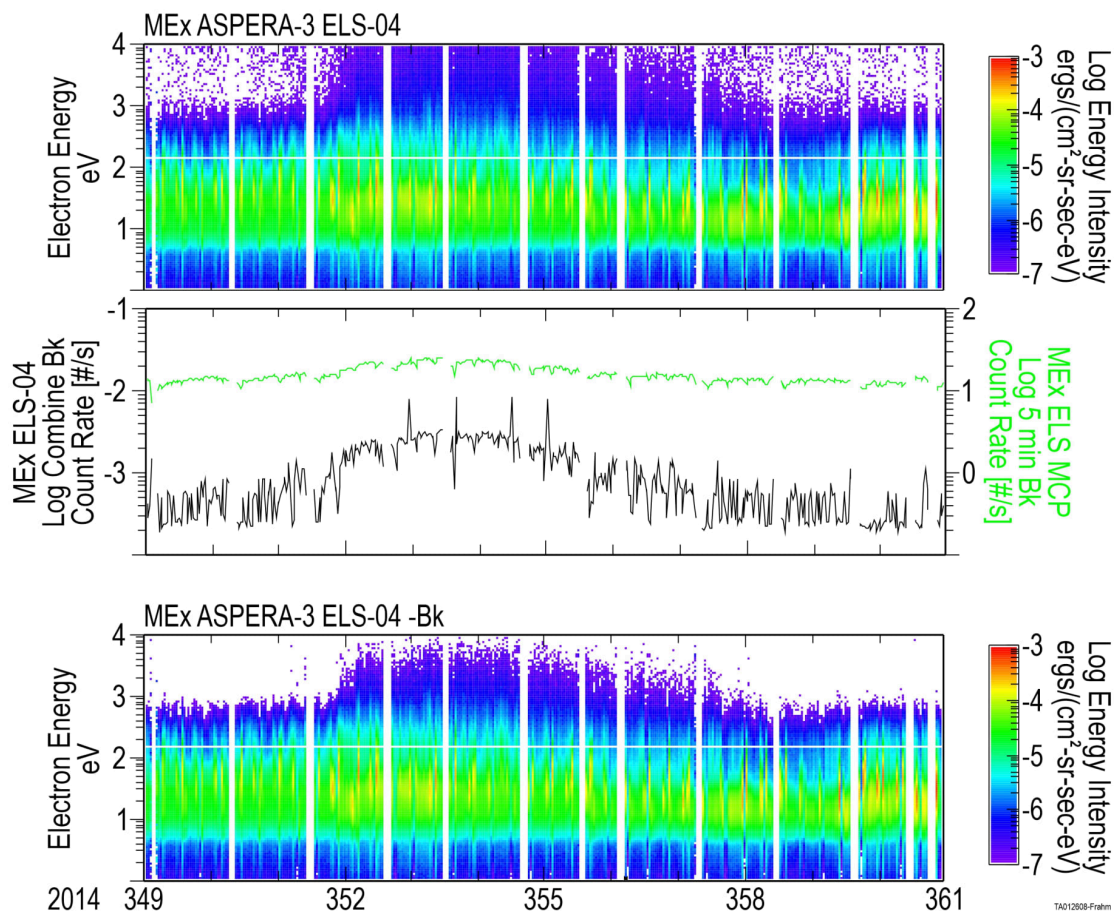


Figure 8. This event in 2014 shows no initial large spike in energy flux as seen in the 2012 (Figure 6) and 1011 (Figure 7) events, but more of a gradual rise and then fall in the energy and energy flux, both in the solar wind and in the Mars magnetosheath. The format is the same as in Figure 6.

Storms are not restricted to single events. Figure 9 shows multiple events occurring in 2024. There is an increase in solar wind energy flux on 14 May (day 135) where there is not a large increase in the Mars magnetosheath flux, but there was enough high energy penetration to cause an increase in the background level, similar to Figure 8. Then there is another similar event beginning on 17 May (day 138) where there was a large increase in magnetosheath energy flux at Mars. This is followed by an SEP event on May 20 (day 141) which is similar to the 2012 event (Figure 6); however, the decrease in solar wind energy flux almost disappears during the event. The Mars magnetosheath is still observed, driven by lower energy flux at Mars.

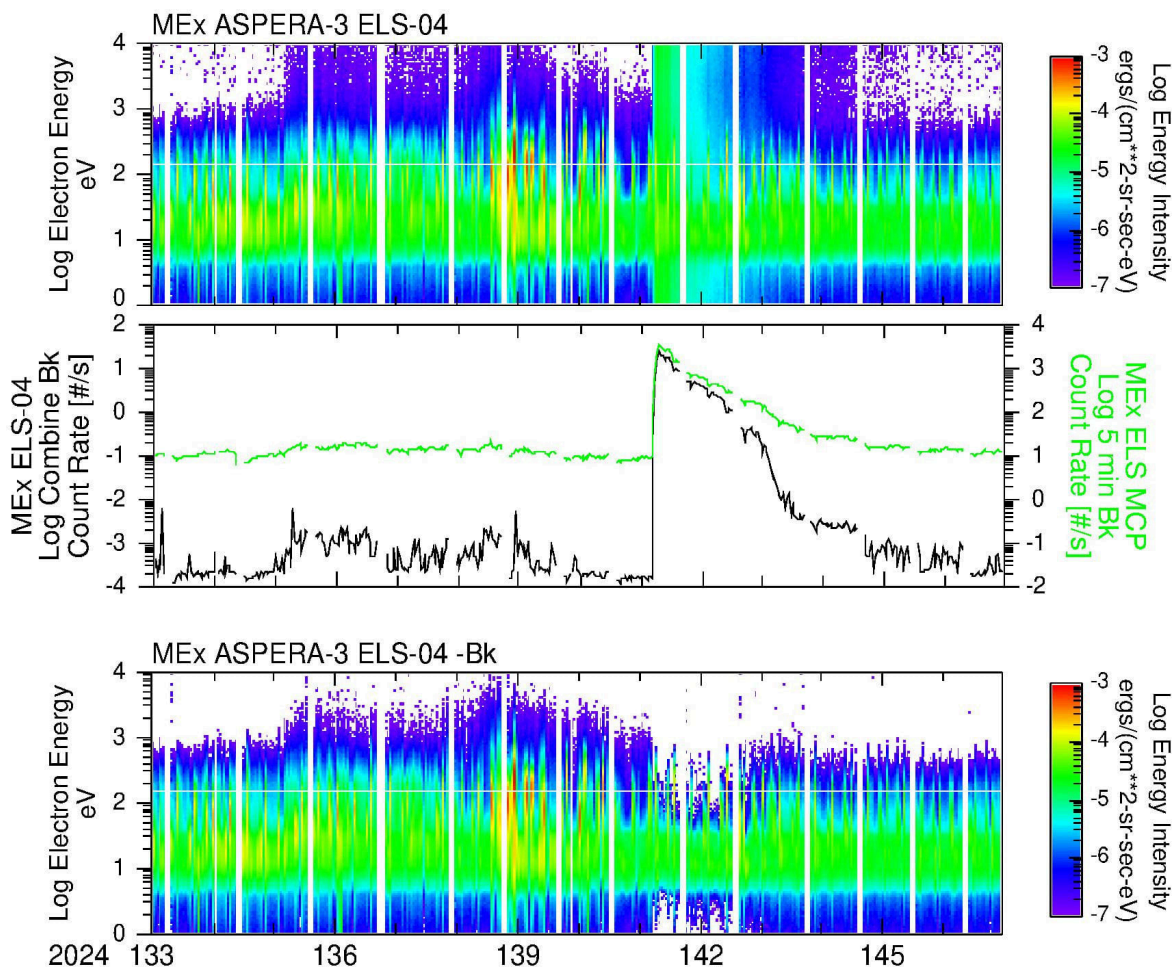


Figure 9. Multiple events occurred in succession in 2024 which had a distinct influence on the Mars magnetosheath, increasing in energy flux during the second event and decreasing in solar wind energy flux during the third event. The third event has a similar characteristic shape to the 2012 SEP event shown in Figure 6. The format is the same as in Figure 6.

One might ask whether background subtraction during times when there is no plasma storm or an increase in solar wind flux should be performed. Figure 10 shows a time in 2019 when the conditions in the solar wind at Mars are normal. Under these conditions, energy below 1 keV shows the signal of the environment around and near the planet. Background levels are observed above 10 keV and are mainly caused by galactic cosmic rays (GCRs). The GCRs cause an energy independent signal in the instrument and generate artificial counts. To reveal the plasma at Mars without the GCR background, the science data should still remove the background to determine the true environmental signal of electrons at Mars.

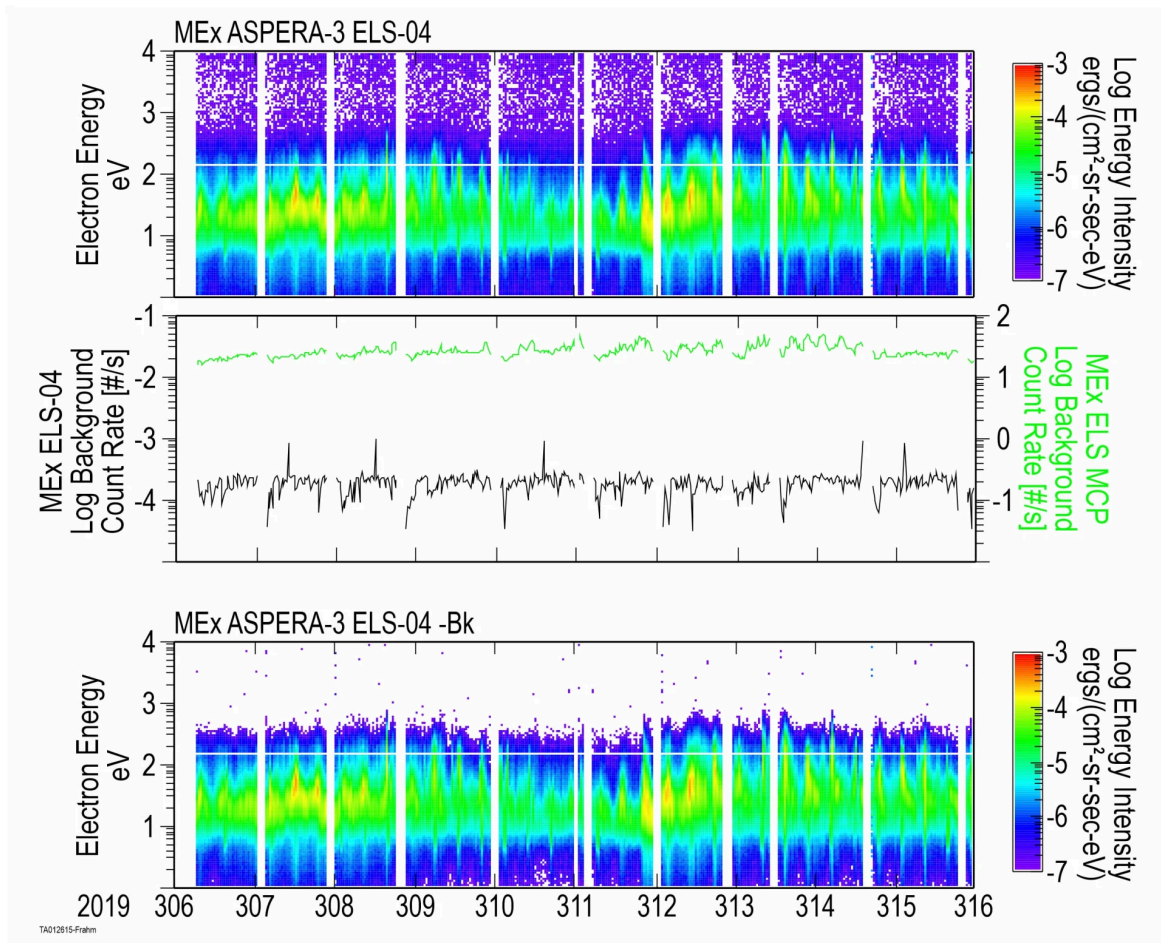


Figure 10. A normal period at Mars showing energy flux below 1 keV in 2019. There are still signals above 10 keV that are caused by galactic cosmic rays which penetrate the sides of the instrument and cause an energy independent signal. Background counts still need to be removed from this data. The format is the same as in Figure 6.

CONCLUSION

Conclusion

The removal process for MEx ELS background has been defined and four different time cadence levels have been developed. These are at the 4-second instrument sweep period, a 1-minute average, a 5-minute average, and a 25-minute average. Each type of background removal is designed for a specific purpose which depends on the rate of variability of the science feature being studied. By awarding this ROSES PDART, NASA shows agreement that the Mars Express ELS background data product is scientifically useful and should be archived.

The ELS Background data has been shown to remove stray signals caused by energy independent features. These include high energy particles from SEP events, GCRs, and X-rays which penetrate the walls of the detector, MCP thermal noise, and electronic noise. Background is predetermined based on the science data and combined to form a multi-time resolution combined background product which is sector dependent. This combined background data will be archived at the NASA PDS PPI node. In fact, all background data – all the different time-resolution background components – as well as the background-corrected science data, will be archived in PDS-4 compliant data files. Data release is expected to occur in mid-to-late 2026.

Removal of background corrects the energy spectrum to eliminate sources of energy independent contamination. Observations during SEP events show that the shape and character of Mars electrons present different time profiles from each other when the SEPs encounter Mars.

DISCLOSURES

We are grateful to NASA for recognizing the importance of this set of data to the analysis of Mars Express ELS measurements and its belief that this set of data will be a benefit to the Science Community. This work was supported by NASA PDART grant 80NSSC24K0797.

AUTHOR INFO

Rudy A. Frahm <rfracm@swri.edu>

Sandee J. Jeffers <sjeffers@swri.org>

Carrie A. Gonzalez <cgonzalez@swri.prg>

TRANSCRIPT

ABSTRACT

There are times when penetrating radiation increases, causing the background level of the electron spectrometer (ELS) to increase on the Mars Express (MEx) spacecraft, which is part of the Analyzer of Space Plasmas and Energetic Atoms (ASPERA-3) experiment. Most notably, this occurs during Solar Energetic Proton (SEP) events. Spectral distortion occurs which hides the actual electron spectrum as the signal becomes dominated by radiation penetrating the spectrometer, masking the true environmental electron spectrum. Due to the small geometric factor of the electron spectrometer, environmental signals are rarely observed above 10 keV. These measurements are used to determine the instrument background. Since this background is energy independent, the measurement above 10 keV can be used to correct the electron spectrum below 10 keV and reveal the real spectral impact of the SEP event on the Mars environment. This technique can be used to correct the electron spectrum during any energy independent noise event, such as temperature related sensor noise, electronic noise, or in some cases, interference from the spacecraft or other instrument related signal coupling. During some geophysical events, this background level is observed to increase, making background removal from lower energies relevant to recovery of the Martian electron spectrum. The NASA Planetary Data System (PDS) has decided that it is worthy to archive the MEx ELS background data so that it is publicly accessible; however, several background values will be used to determine the best representation for background removal on a sector and time basis. The background data and correct electron spectra will be archived in the NASA PDS.

Plain-Language Summary

A Solar Energetic Proton (SEP) event is highly energetic and places energy deep in the atmosphere of Mars. An SEP event can penetrate through the walls of the electron detector on the Mars Express (MEx) spacecraft. This leads to a contaminated electron spectrum and hides the environment event signal so that determination of the reaction of the Mars environment at time of the SEP is masked. A technique is presented to recover the electron spectrum, revealing the environment behavior during the SEP.

REFERENCES

- Barbash, S. R. Lundin, H. Andersson, J. Gimholt, M. Holmström, O. Norberg, M. Yamauchi, K. Asamura, A. J. Coates, D. R. Linder, D. O. Kataria, C. C. Curtis, K. C. Hsieh, B. R. Sandel, A. Fedorov, A. Grigoriev, E. Budnik, M. Grande, M. Carter, D. H. Reading, H. Koskinen, E. Kallio, P. Riihelä, T. Säles, J. Kozyra, N. Krupp, S. Livi, J. Woch, J. Luhmann, S. McKenna-Lawlor, S. Orsini, R. Cerulli-Lrelli, M. Maggi, A. Morbidini, A. Mura, A. Milillo, E. Roelof, D. Williams, J.-A. Sauvaud, J.-J. Thocaven, T. Moreau, D. Winningham, R. Frahm, J. Scherrer, J. Sharber, P. Wurz, and P. Bochsler, "ASPERA-3: Analyser of Space Plasmas and Energetic Ions for Mars Express," in **MARS EXPRESS: The Scientific Payload** (<https://sci.esa.int/web/mars-express/-/34885-esa-sp-1240-mars-express-the-scientific-payload>), ed. A Wilson, European Space Agency Publications Division, European Space Research & Technology Centre, Noordwijk, The Netherlands, SP-1240, 121-139, 2004.
- Barabash, S., R. Lundin, H. Andersson, K. Brinkfeldt, A. Grigoriev, H. Gunell, M. Holmström, M. Yamauchi, K. Asamura, P. Bochsler, P. Wurz, R. Cerulli-Irelli, A. Mura, A. Milillo, M. Maggi, S. Orsini, A. J. Coates, D. R. Linder, D. O. Kataria, C. C. Curtis, K. C. Hsieh, B. R. Sandel, R. A. Frahm, J. R. Sharber, J. D. Winningham, M. Grande, E. Kallio, H. Koskinen, P. Riihelä, W. Schmidt, T. Säles, J. U. Kozyra, N. Krupp, J. Woch, S. Livi, J. G. Luhmann, S. McKenna-Lawlor, E. C. Roelof, D. J. Williams, J.-A. Sauvaud, A. Fedorov, and J.-J. Thocaven, "The Analyzer of Space Plasmas and Energetic Atoms (ASPERA-3) for the Mars Express Mission (<https://link.springer.com/article/10.1007/s11214-006-9124-8>)", *Space Science Reviews*, **126**, 113-164, 2006.
- Delory, G. T., J. G. Luhmann, D. Brain, R. J. Lillis, D. L. Mitchell, R. A. Mewaldt, and T. V. Falkenberg, "Energetic particles detected by the Electron Reflectometer instrument on the Mars Global Surveyor, 1999-2006," *Space Weather*, **10**, S06003, doi:10.1029/2012SW000781 (<https://agupubs.onlinelibrary.wiley.com/doi/10.1029/2012SW000781>), 2012.
- Duru, F., D. A. Gurnett, D. D. Morgan, J. Halekas, R. A. Frahm, R. Lundin, W. Dejong, C. Ertl, A. Venable, C. Wilkinson, M. Fraenz, F. Nemeč, J. E. P. Connerney, J. R. Espley, D. Larson, J. D. Winningham, J. Plaut, and P. R. Mahaffy, "Response of the Martian Ionosphere to Solar Activity including SEPs and ICMEs in a two week period starting on 25 February 2015," *Planetary and Space Science*, **145**, 28-37, doi:10.1016/j.pss.2017.07.010, (<https://www.sciencedirect.com/science/article/pii/S0032063316304329>) 2017.
- Duru, F., R. A. Frahm, D. Hughes, T. Caplice, J. Pierce, and H. Madanian, Local electron density depletions in the Martian upper ionosphere obtained from MARSIS: Comparison with ASPERA-3, and MAVEN, and the connection with crustal magnetic fields, *Journal of Geophysical Research*, **128**, e2023JA031327, <https://doi.org/10.1029/2023JA031327> (<https://doi.org/10.1029/2023JA031327>), 2023.
- Frahm, R. A., J. R. Sharber, J. D. Winningham, H. A. Elliott, T. A. Howard, C. E. DeForest, D. Odstrčil, E. Kallio, S. McKenna-Lawler, and S. Barabash, "Solar energetic particle arrival at Mars due to the 27 January 2012 solar storm," *Solar Wind 13*, **AIP Conf. Proc.** **1539**, 394-397, doi:10.1063/1.4811068 (<https://pubs.aip.org/aip/acp/article/1539/1/394/878511/Solar-energetic-particle-arrival-at-Mars-due-to>), 2013a.
- Frahm, R. A., J. R. Sharber, J. D. Winningham, H. A. Elliott, T. A. Howard, C. E. DeForest, D. Odstrčil, E. Kallio, S. McKenna-Lawler, and S. Barabash, "The coronal mass ejection interaction with the induced magnetosphere of Mars due to the 27 January 2012 solar storm," *Solar Wind 13*, **AIP Conf. Proc.** **1539**, 398-401, doi:10.1063/1.4811069 (<https://doi.org/10.1063/1.4811069>), 2013b.
- Frahm, R. A., J. D. Winningham, A. J. Coates, J.-C. Gérard, M. Holmström, and S. Barabash, "The largest electron differential energy flux observed at Mars by the Mars Express spacecraft 2004-2016," *Journal of Geophysical Research*, **123**, doi:10.1029/2018JA025311 (<https://doi.org/10.1029/2018JA025311>), 2018.
- Frahm, R. A., Venus Express ASPERA-4 ELS Background Data Examples, NASA Planetary Data System, Planetary Plasma Interactions node, <https://doi.org/10.17189/5myh-dg54> (<https://doi.org/10.17189/5myh-dg54>), 2021.
- Harada, Y., Y. Fujiwara, R. J. Lillis, J. Deighan, H. Nakagawa, B. Sanchez-Cano, M. Lester, Y. Futaana, M. Holmstrom, and R. A. Frahm, Discrete aurora and the nightside ionosphere of Mars: an EMM-MEX conjunction of FUV imaging, ionospheric radar sounding, and suprathermal electron measurements, *Earth Planets Space*, **76**, 64, <https://doi.org/10.1186/s40623-024-02010-x> (<https://doi.org/10.1186/s40623-024-02010-x>), 2024.

Madanian, H., T. Hesse, F. Duru, M. Pilinski, and R. A. Frahm, Ionospheric density depletions around crustal fields at Mars and their connection to ion frictional heating, *Annales Geophysicae*, **42**, 69–78, <https://doi.org/10.5194/angeo-42-69-2024> (<https://angeo.copernicus.org/articles/42/69/2024/angeo-42-69-2024.html>), 2024.

Möstl, C., T. Rollett, R. A. Frahm, Y. D. Liu, D. M. Long, R. C. Colaninno, M. A. Reiss, M. Temmer, C. J. Farrugia, A. Posner, M. Dumbović, M. Janvier, P. Démoulin, P. Boakes, A. Devos, E. Kraaikamp, M. L. Mays, B. Vršnak, “Strong coronal channeling and interplanetary evolution of a solar storm up to Earth and Mars,” *Nat. Comm.*, **7**, 7135, doi:10.1038/ncomms8135 (<https://www.nature.com/articles/ncomms8135>), 2015.

Posner, A., D. Odstrčil, P. MacNeice, L. Rastaetter, C. Zeitlin, B. Heber, H. Elliott, R. A. Frahm, J. J. E. Hayes, T. T. von Roseninge, E. R. Christian, J. P. Andrews, R. Beaujean, S. Böttcher, D. E. Brinza, M. A. Bullock, S. Burmeister, F. A. Cucinotta, B. Ehresmann, M. Epperly, D. Grinspoon, J. Guo, D. M. Hassler, M.-H. Kim, J. Köhler, O. Kortmann, C. Martin Garcia, R. Müller-Mellin, K. Neal, S. C. R. Rafkin, G. Reitz, L. Seimetz, K. D. Smith, Y. Tyler, E. Weigle, and R. F. Wimmer-Schweingruber, “The Hohmann-Parker effect measured by the Mars Science Laboratory on the transfer from Earth to Mars: Consequences and opportunities,” *Planetary and Space Science*, **89**, 127-139, doi:10.1016/j.pss.2013.09.013 (<https://www.sciencedirect.com/science/article/pii/S0032063313002407>), 2013.

Rollett, T., C. Möstl, M. Temmer, R. A. Frahm, J. A. Davies, A. M. Veronig, B. Vršnak, U. V. Amerstorfer, C. J. Farrugia, T. Žic, and T. L. Zhang, “Combined Multipoint Remote and In Situ Observations of the Asymmetric Evolution of a Fast Solar Coronal Mass Ejection,” *Astrophysical Journal Letters*, **790**:L6 (7pp), doi:10.1088/2041-8205/790/1/L6 (<https://iopscience.iop.org/article/10.1088/2041-8205/790/1/L6>), 2014.

EVALUATIONS

#	Average Score
<p data-bbox="293 283 581 380">There are currently no completed evaluations for this presentation</p>	

+